Frequency-dependent jet noise source localization using cross-correlation between near and far-field microphone arrays

Jacob A. Ward, S. Hales Swift, Kent L. Gee, Tracianne B. Neilsen, Koji Okamoto, and Masahito Akamine

Citation: Proc. Mtgs. Acoust. **31**, 040005 (2017); doi: 10.1121/2.0000810
View online: https://doi.org/10.1121/2.0000810
View Table of Contents: http://asa.scitation.org/toc/pma/31/1
Published by the Acoustical Society of America

Proceedings of Meetings on Acoustics

Volume 31 http://acousticalsociety.org/

174th Meeting of the Acoustical Society of America

New Orleans, Louisiana

04-08 December 2017

Noise: Paper 1pNS9

Frequency-dependent jet noise source localization using cross-correlation between near and far-field microphone arrays

Jacob A. Ward, S. Hales Swift, Kent L. Gee and Tracianne B. Neilsen
Physics and Astronomy Department, Brigham Young University, Provo, UT, 84602; jacob.ward@live.com; hales.swift@gmail.com; kentgee@byu.edu, tbn@byu.edu

Koji Okamoto and Masahito Akamine
Department of Advanced Energy, University of Tokyo, Kashiwa, 277-0882, JAPAN; k-okamoto@k.u-tokyo.ac.jp; akamine@thermo.t.u-tokyo.ac.jp

The apparent acoustic source region of jet noise varies as a function of frequency. In this study, the variation of the apparent maximum source location with frequency is considered for an ideally expanded, unheated, Mach-1.8 jet with exit diameter of 20 mm. In this study, the source location is ascertained for one-third octave bands by evaluating peak cross-correlation between near-field linear microphone arrays at three side-line distances and a far-field microphone arc. The impact of the hydrodynamic field on correlation results is considered. Source locations determined by these means are compared with intensity analyses for the same jet [K. L. Gee et al., AIAA Paper 2017-3519 (2017)]. Correlational methods together with filtering can provide a straightforward measure of the acoustic origin as a function of frequency and thus inform optimal microphone array layout for specific frequency regimes.

Published by the Acoustical Society of America

 https://doi.org/10.1121/2.0000810

1. INTRODUCTION

Spatio-temporal analyses of jet noise data have been previously used to gain physical insights into the aeroacoustic sources.[1,2] By examining the radiated sound field, jet noise-source characteristics, such as the apparent acoustic source region, can be obtained.[3] Previous experiments using methods such as beamforming,[4–6] acoustic intensity analyses,[7] and near-field acoustical holography[8–13] have shown that the apparent downstream distance of the acoustic source region varies with frequency. The present analysis presents a straightforward method for analyzing the frequency-dependent nature of the source that utilizes band-passed cross-correlation between a near-field line array and a far-field arc. Previous studies have shown that microphones in the near field sense the pressure fluctuations of the turbulent hydrodynamic near field in addition to propagating acoustical pressure fluctuations.[14,15] The effect of the hydrodynamic near field is therefore also investigated as it dramatically affects results.

2. EXPERIMENT

This experiment was completed in a jet facility located at the Hypersonic High-enthalpy Wind Tunnel at the Kashiwa Campus of the University of Tokyo. In the present experiment, the unheated Mach 1.8 laboratory-scale jet was ideally expanded through a 20-mm diameter converging-diverging nozzle. Due to the non-anechoic nature of the facility, nearby reflecting surfaces were covered with fiberglass. Akamine *et al.*[16] showed that this produced favorable matches to anechoic measurements by Greska.[17]

Time-series data from 32 microphones were simultaneously recorded using NI PXI-4498 cards at a sampling rate of 204.8 kHz. As shown in Figure 1, the microphone setup consisted of a stationary 16-channel polar microphone arc with 5°spacing and a 16-channel near-field line array with 1 nozzle diameter (D) spacing fitted with an automated positioning system to allow it to be moved to various downstream and sideline distances. The arc microphones were positioned 40D away from the measurement array reference point which is 10D downstream from the jet exit. The line array was moved to three different sideline distances, namely 2.5, 5, and 10D from the jet centerline. At each of these sideline distances the line array was moved to three different downstream positions, the first covering 0 to 15D downstream, the second covering 10 to 25D downstream, and the third covering 18 to 33D downstream. At each position, the noise was measured for 6 seconds before the line array moved to the next location. By including overlap between the downstream positions, the experiment naturally includes some data redundancy as well as opportunities for data verification.

3. SPATIO-TEMPORAL ANALYSES

A. BAND-PASSED CROSS-CORRELATION

In order to determine the locations of the frequency-dependent apparent acoustic source region, the main analysis approach taken here involves evaluating the cross-correlation between the signals picked up by the microphones on the line array and those picked up by the microphones on the arc array. Looking at the cross-correlation for various combinations of microphones on the line and arc arrays, the characteristics of the fine-scale and large-scale turbulent structure noise that have been

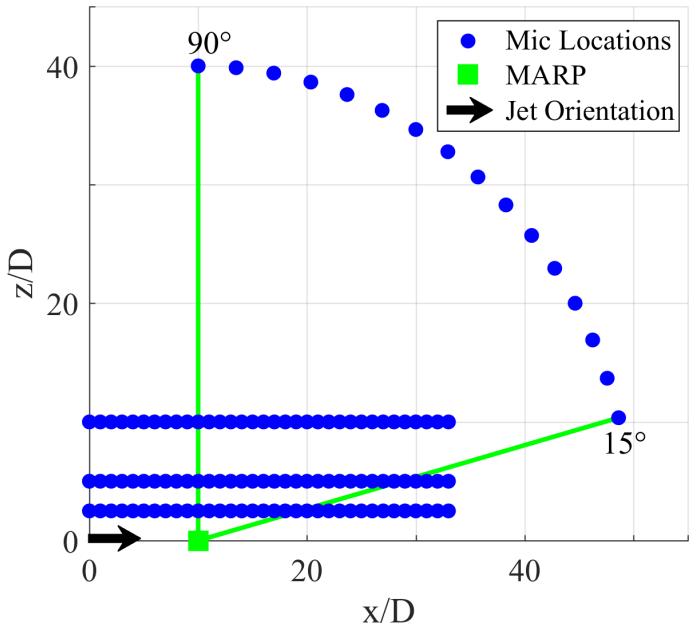

Figure 1: Experimental setup showing microphone locations in relation to jet. Arc microphone angles are relative to the microphone array reference point (MARP) 10 jet nozzle diameters downstream.

shown in previous work to dominate in the sideline and aft directions respectively[18] are evident. For instance, Figure 2 shows the cross-correlation between the microphones on the z = 5D array with the arc microphone at 90°(left) and the arc microphone at 30°(right). The 90°arc microphone, which is in the sideline region that is known to be dominated by fine-scale turbulence,[19] shows very little correlation with the 5D array with a maximum peak correlation of just over 0.1. Conversely, the arc microphone 30°above the jet exhaust, which is in the Mach-wave radiation region known to be dominated by large-scale turbulent structure noise,[19] shows significant peak correlations in excess of 0.7 in some cases. Significant correlation of over 0.4 is seen over an axial extent of 14D. The correlation coefficients from every combination of arc and line array microphones can be analyzed in order to identify the axial and angular extent over which significant correlation exists between the arc and line microphone arrays.

Because the peak cross-correlation coefficients are the only data of interest in the present investigation, the time delay information is neglected and peak cross-correlation coefficient maps are created for each line array/arc array combination. An example of such a map is seen in Figure 3, which shows the map for the 2.5D array correlated with the arc array. Any point on a given map gives the peak cross-correlation coefficient for the arc microphone angle specified by the y-axis in degrees above the jet exhaust and the line array microphone position specified by the x-axis in D downstream from the jet nozzle. Visualizing the cross-correlation data in this manner, the axial and angular extent to which there is significant correlation can be easily seen. The dotted red lines on the coefficient maps and the red-shaded region on the experiment geometry plot have been added as an aid in understanding where the general correlated region is located spatially but do not represent any specific numerical boundary.

Performing the same cross-correlation using band-passed signals gives insight into how the

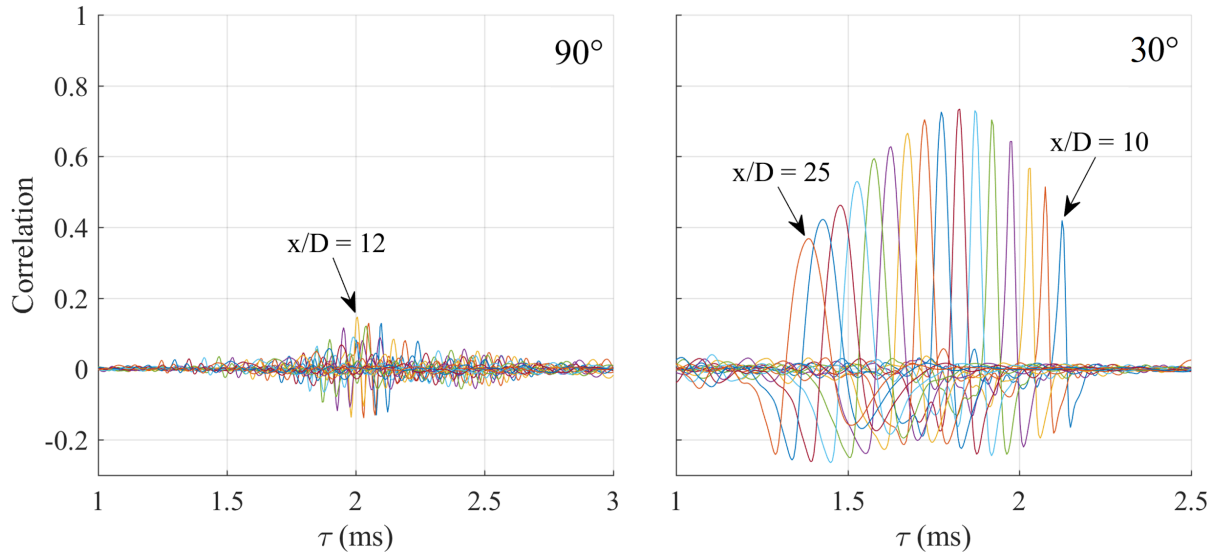

Figure 2: Cross-correlation between the 5D line array microphones and the arc microphones at a) 90°and b) 30°.

correlated region changes with frequency. Figure 4 shows the peak cross-correlation coefficient maps for various frequencies. Several behaviors are noticed as the frequency increases from 5 kHz to 20 kHz (St=0.205 to St=0.820) that should be pointed out: 1) the correlated region moves upstream on the line array, 2) the correlated region moves to slightly greater angles on the arc array, and 3) the overall correlation decreases. As the estimated source region is determined using these maps, these differences between frequencies correspond to the differences in traced source regions that are addressed in the following section.

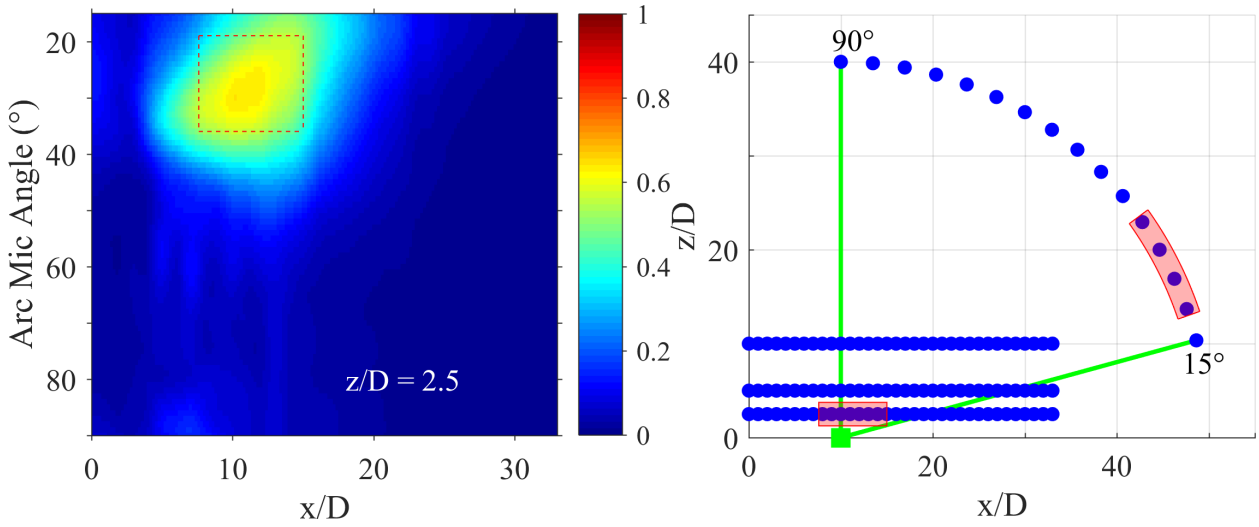

Figure 3: (Left) Peak coefficient maps for cross-correlation between the 2.5D array and the arc array with the dotted red box corresponding to microphones highlighted in red on the experimental layout (right).

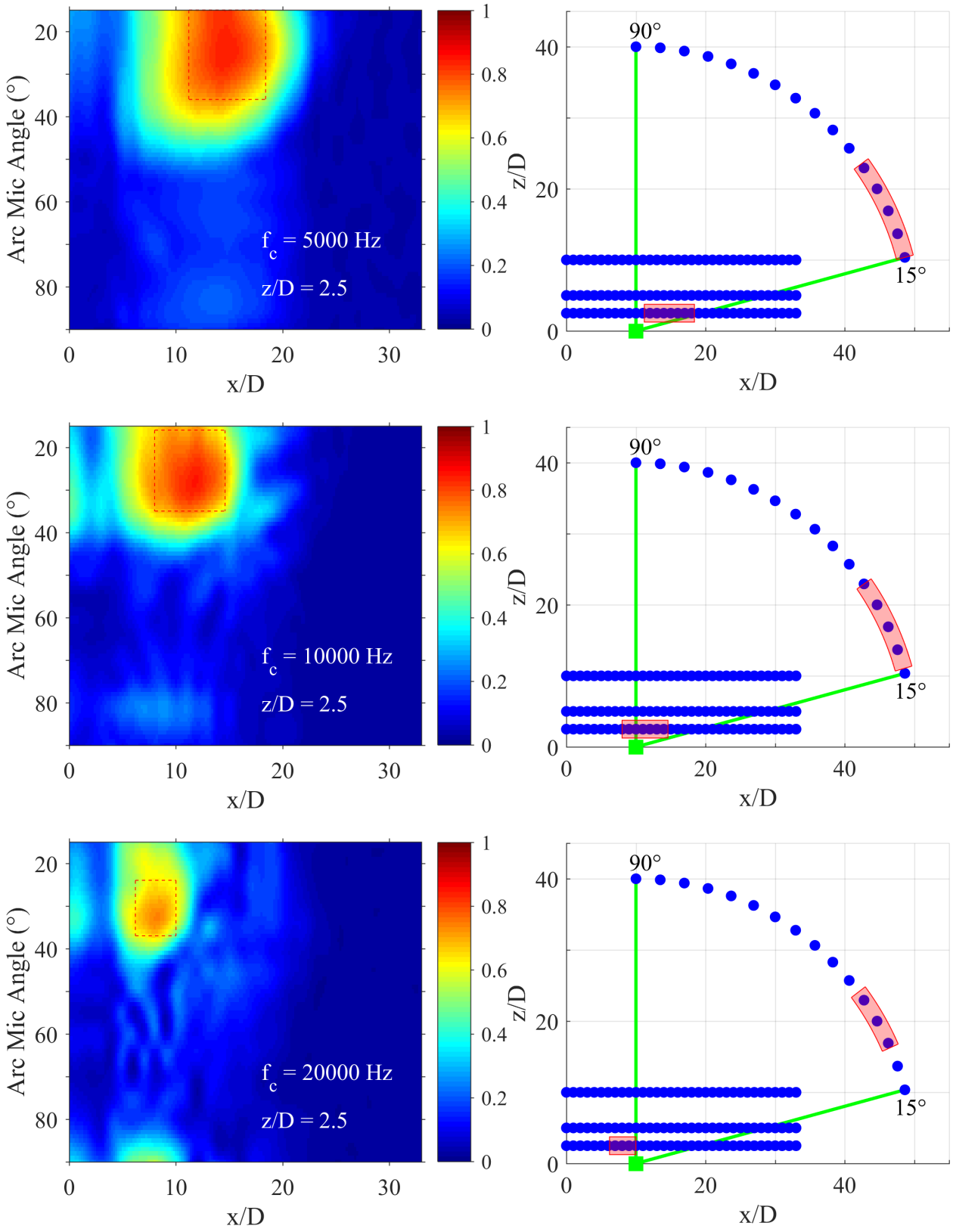

Figure 4: Peak coefficient maps for band-pass filtered cross-correlation between the 2.5D array and the arc array for various frequencies, similar to Figure 3.

B. SOURCE REGION TRACING

Because two different spatial regions are being compared, strong correlation between any two points on the arrays allows a source location to be traced to the jet centerline. For example, using the 10 kHz (St=0.420) map from Figure 4, the maximum point on the map is located at 12D on the line array and at 30°on the arc array. Tracing these two points to the jet centerline gives an approximate source location at around 7D downstream of the jet exit. The process can also be repeated with the 5D line array map. This process is shown in Figure 5 with Figure 5b showing the resulting path traced using both the 2.5D array map and 5D array map. Both maps are consistent in tracing out a point that is around 7D downstream of the jet exit.

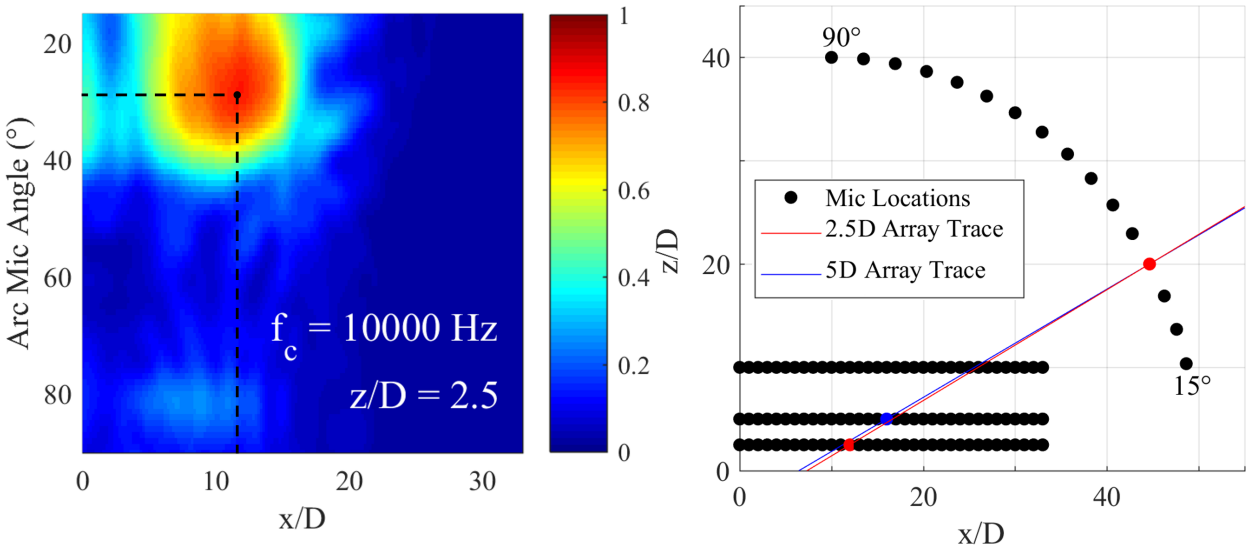

Figure 5: Example of how the maximum value of a band-pass filtered peak coefficient map (left) is used to trace the apparent acoustic source location (right) for center frequency of 10 kHz (St=0.420).

To obtain the source region and not just a source point, ray tracing is applied between arc and line array microphone pairs. Each interpolated arc location with a peak cross-correlation coefficient within 95% of the maximum at each frequency is traced to a line array position. Using the 10 kHz (St=0.420) case again as an example, the result of this tracing is shown in Figure 6. Because the correlation maps have been interpolated, the number of points traced from the arc to the line array exceeds the number of physical microphones present in the experimental setup. This helps to overcome the limitation of only sampling the field at discrete spatial points, especially along the arc where the spatial refinement is considerably lower than along the line arrays.

Following this process for each one-third-octave band frequency from 2 to 40 kHz (St=0.0820 to St=1.64) results in the traced source regions seen in Figure 7 versus frequency. Each green point is a source point traced from a line array/arc array pair where the peak correlation coefficient between the two was within 95% of the maximum peak correlation coefficient. Both the points traced from the 2.5D array map and the 5D array map are shown. Black dots indicate the mean location, and black lines indicate the standard deviation for each frequency. It can be seen that from around 8 kHz (St=0.328) and above, the traced source region is fairly compact and moves

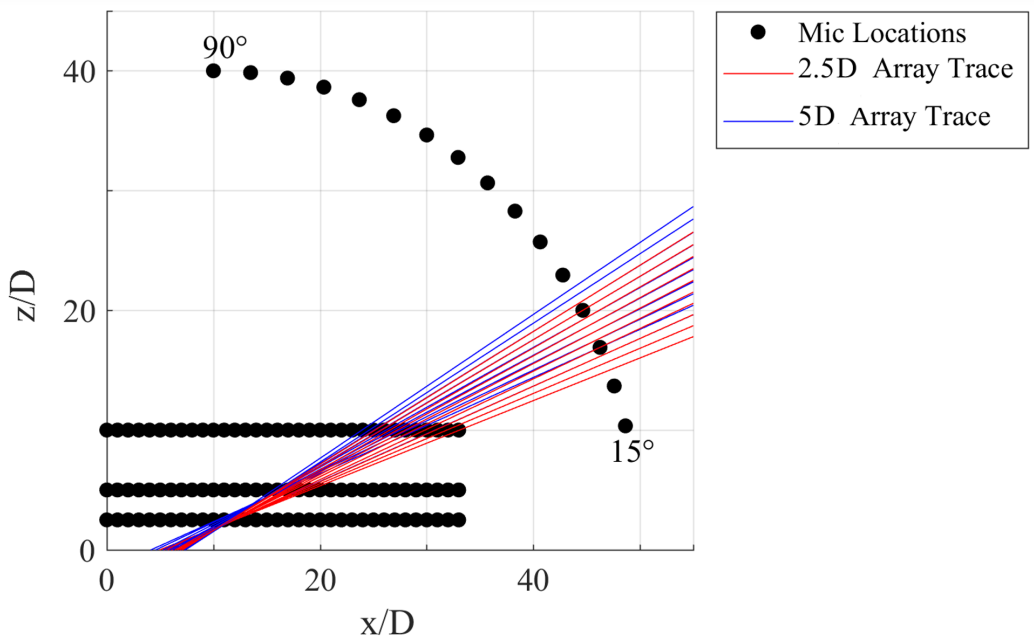

Figure 6: Source tracing of all points within 95% of maximum using band-pass filtered peak cross-correlation maps for the 2.5D and 5D arrays for center frequency of 10 kHz (St=0.420).

upstream with increase in frequency. Below 8 kHz (St=0.328) the source region broadens and the lower standard deviation line and mean points turn around towards the upstream instead of continuing the pattern of moving downstream.

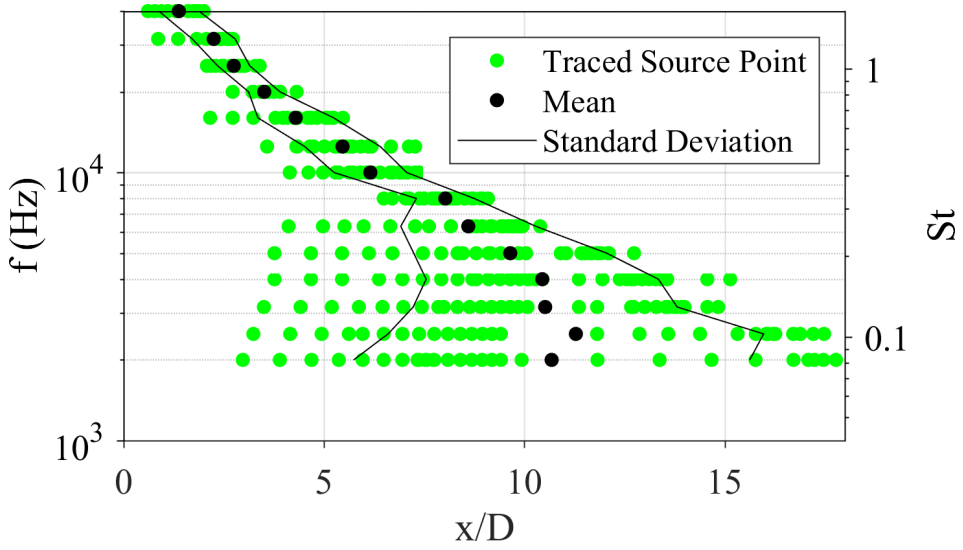

Figure 7: Traced source region versus frequency including all points traced using both the 2.5D and 5D arrays.

4. DISCUSSION

A. COMPARISON TO INTENSITY ANALYSES

In an effort to verify the efficacy of this source tracing process and the validity of the results, the results have been compared to intensity analyses done on the same jet by Gee *et al.*[7] In their analyses, the intensity probes contained three-pressure microphones, and a phase-unwrapping procedure was used to obtain intensity vectors for frequencies up to 40 kHz. Ray tracing was then applied to the intensity vectors to obtain the estimated source region for each frequency (Figure 8 left). The source regions calculated using the peak correlation coefficient method in this paper (Figure 8 right) have been found to be broadly consistent with their prior intensity-based results between 2 kHz and 40 kHz with certain key differences. Below 2 kHz, the presence of two separated peaks in the cross-correlation data (associated with the increased prominence of near-field hydrodynamic pressure contributions) limited our method. Both traced source regions stay fairly compact and move upstream for higher frequencies. Both results also show that as the frequency decreases, there comes a point where the source region widens and turns back toward the upstream. This turnaround behavior is a point of interest and one that can be investigated further using the correlation results.

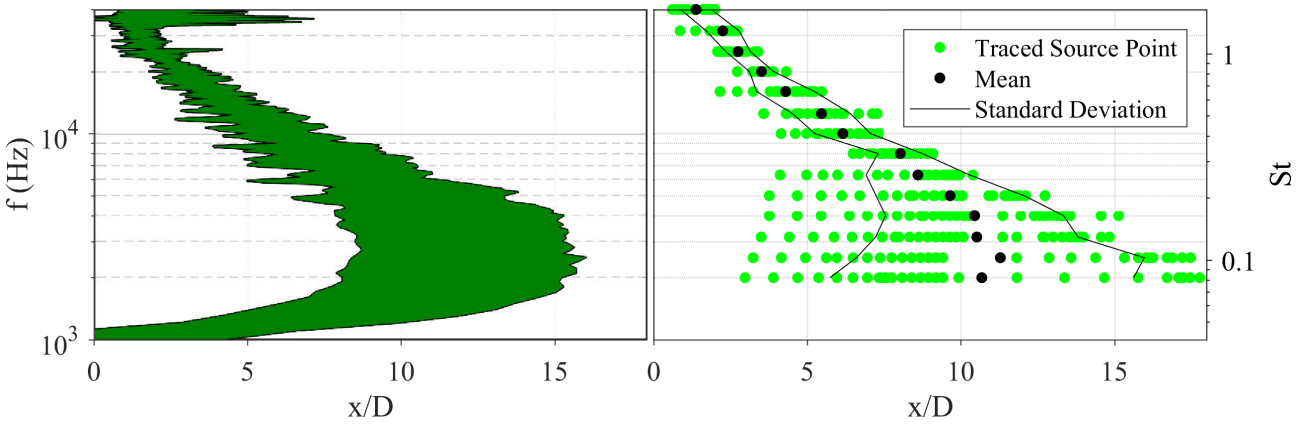

Figure 8: Side by side comparison of the traced source regions from the intensity analyses done by Gee et al.[7] (left) and the present experiment's traced source regions (right).

While combining the source points traced from both the 2.5D and 5D arrays confirms the shape of the intensity analyses results, looking at the individual contributions of both arrays can be instructive as to the cause of the turnaround behavior. In Figure 9, the individual source tracing contributions of both arrays are shown overlaid on the intensity results for comparison. Again, the boundary lines for the regions are the standard deviation for the traced source points. While they agree fairly well for higher frequencies, stark contrasts can be seen in the behavior of the source regions traced by the 2.5D and 5D arrays below 8 kHz (St=0.328). While the 2.5D traced source region turns around and broadens just under 8 kHz (St=0.328), the 5D traced source region continues to stay compact and move downstream until about 2.5 kHz (St=0.102) when it finally starts to widen and turn around as well. In order to explain the differences in behavior below 8 kHz (St=0.328), a brief discussion of the effects of the hydrodynamic near field is helpful.

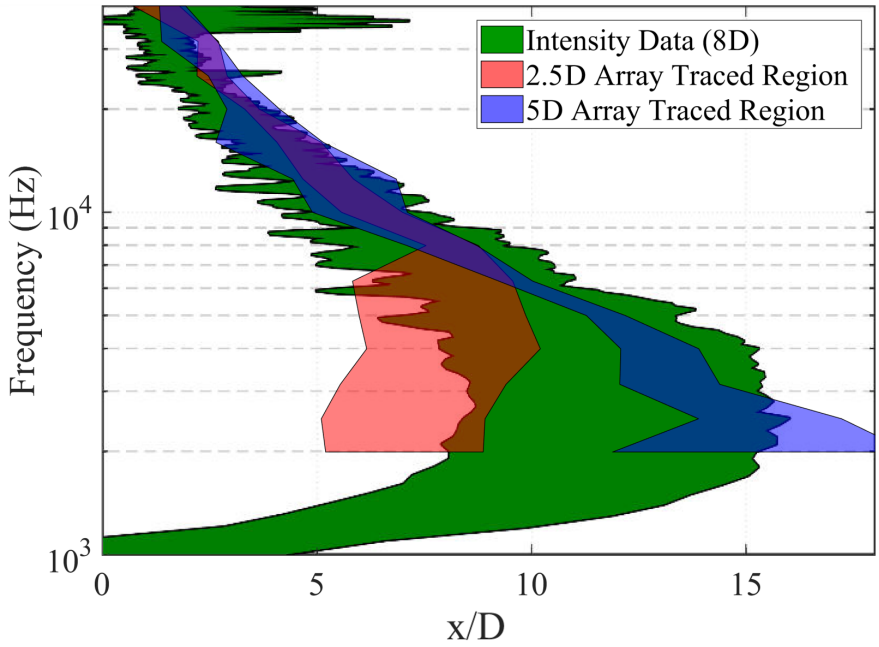

Figure 9: Individual contributions to source tracing of the 2.5D and 5D arrays overlaid on intensity analyses results for comparison.

B. HYDRODYNAMIC NEAR FIELD

Hydrodynamic near-field noise is an especially important factor to consider when dealing with near-field arrays close to the jet centerline. Hydrodynamic near-field noise is characterized as being primarily low-frequency content[15,20] that is nonpropagating, sometimes referred to as pseudosound.[15,21] As such, it is largely uncorrelated with the propagated sound field away from the jet centerline. It is instead present at locations near the jet shear layer. The jet shear layer expands linearly with distance from the jet nozzle. The mixing jet thus grows in radius with downstream distance so that hydrodynamic effects are observable farther from the centerline at positions farther downstream. The spectra for the 2.5D, 5D, and 10D arrays allows the hydrodynamic regime to easily be seen. In Figure 10, the spectra for the 2.5D array shows a boost of low-frequency content in the range of 10 to 33D downstream, while the 5D array shows a smaller boost of low-frequency content in the range of 15 to 33D downstream, and the 10D array exhibits very little signs of hydrodynamic influence in terms of spectral content at only the farthest downstream locations. The spectra tell us that the hydrodynamic field affects the 2.5D array much farther upstream than the 5D array which is consistent with the fact that the traced source region for the 2.5D array expands and turns around much farther upstream than the traced source region for the 5D array. The turnaround and apparent broadening of the source extent with decreased frequency thus seems to be due to the presence of the hydrodynamic near field.

When looking at the frequencies at which hydrodynamic influence is seen in the spectra, the 2.5D array shows the hydrodynamic component dominates at frequencies less than 10 kHz (St=0.420) especially at the furthest downstream parts of the array. Around 8 kHz (St=0.328), the hydrodynamic spectral contribution competes with the acoustical signal at the part of the array receiving the most significant part of the acoustic energy and thus effects tracing. At the 5D array,

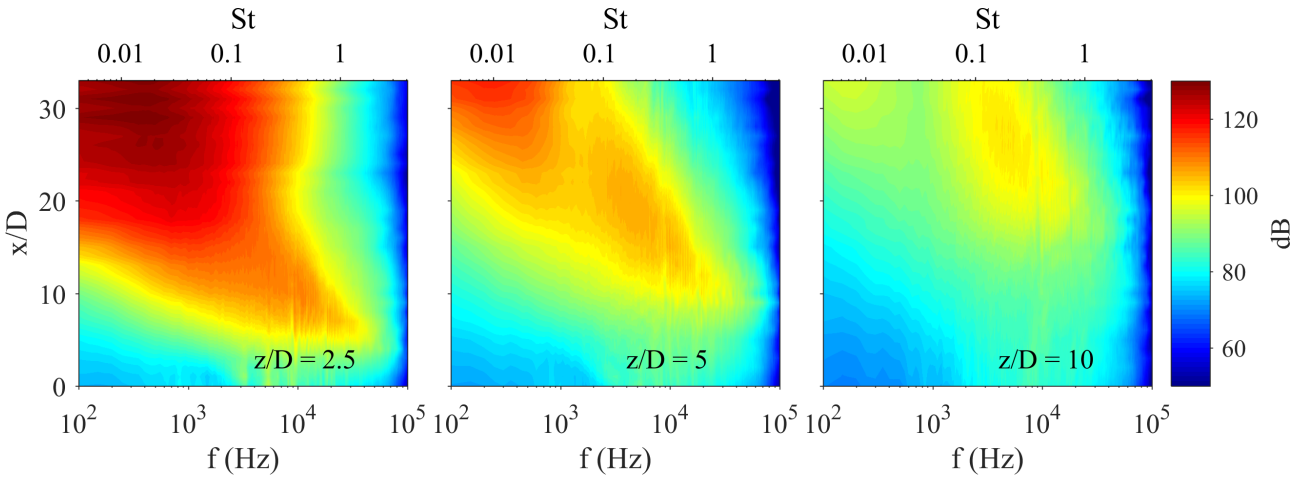

Figure 10: Spectra of the 2.5D, 5D, and 10D arrays versus downstream distance.

the hydrodynamic component dominates at frequencies lower than 2 kHz (St=0.0820), where jet mixing noise contributions are less prominent, as can be seen in the spectra. The frequencies at which the turnaround occurs are thus also consistent with the frequencies at which hydrodynamic effects are prominent in the spectra.

Another characteristic that can be investigated in order to examine the influence of the hydrodynamic near field are the trends in overall correlation versus frequency. In correlation analyses done by Viswanathan[1] on heated and unheated jets of various Mach numbers, he found that moving his microphone arrays closer to the jet centerline resulted in a drop in overall correlation with the far field, presumably due to the influence of the hydrodynamic near field. This drop in correlation, particularly at low frequencies, is apparent in the cross-correlation data for this experiment. Figure 11 shows the maximum peak cross-correlation coefficient for each frequency using the 2.5D array, 5D array, and 10D array.

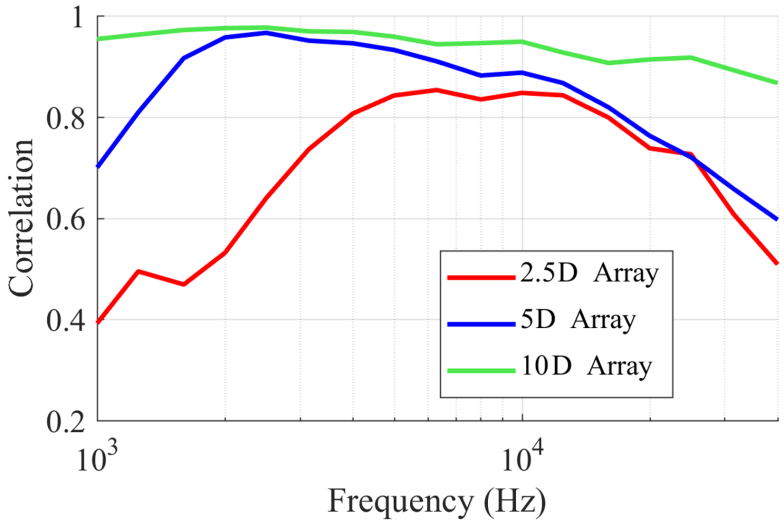

Figure 11: Maximum peak cross-correlation coefficient for each frequency for the 2.5D, 5D, and 10D arrays.

Starting with 40 kHz (St=1.64) and moving down in frequency, all three arrays follow similar trends of increasing maximum correlation coefficients as frequency decreases; however, the 2.5D and 5D arrays see a leveling off and rapid drop in maximum correlation coefficients at around 7 kHz (St=0.287) and 2.5 kHz (St=0.102) respectively. It should be noted that the frequencies at which significant drops in overall correlation are seen on the 2.5D and 5D arrays align fairly well with the frequencies at which we see the traced source region widen and turn around in Figure 9 as well as the frequencies in the spectra where substantial hydrodynamic components are seen. That the drop in correlation coincides with the frequency of turning in the traced source region between the 2.5D and 5D array and matches the approximate upper frequency boundary of the hydrodynamic near-field contributions at each line array is strong evidence that this change in the estimated source region is directly due to the influence of the hydrodynamic near field.

5. CONCLUSION

A method has been presented to determine the frequency-dependent apparent acoustic source region of jet noise using band-passed cross-correlation between several near-field line arrays and a far-field arc. The method's effectiveness has been confirmed by comparison with source region estimates obtained from intensity analyses done on the same jet. It has also been shown that the near-field array's proximity to the jet centerline greatly influences locations of the traced source region due to the greater effect of hydrodynamic near-field noise at smaller sideline distances.

REFERENCES

[1] K. Viswanathan, J. R. Underbrink, and L. Brusniak, " Space-time correlation measurements in near fields of jets," AIAA J. **49**, 1577-1599 (2011).

[2] B. M. Harker, T. B. Neilsen, K. L. Gee, A. T. Wall, and M. M. James, " Spatiotemporal-correlation analysis of jet noise from a high-performance military aircraft," AIAA J. **54**, 1554-1566 (2016).

[3] M. J. Fisher, M. Harper-Bourne, and S. A. L. Glegg, " Jet engine noise source location: The polar correlation technique," J. Sound Vib. **51**, 23-54 (1977).

[4] J. Bridges and L. Sang, " Phased-array measurements of single flow hot jets," AIAA Paper 2005-2842 (2005).

[5] S. S. Lee and J. Bridges, " Phased-array study of dual-flow jet noise: Effect of nozzles and mixers," AIAA Paper 2006-2647 (2006).

[6] B. M. Harker, K. L. Gee, T. B. Neilsen, A. T. Wall, and M. M. James, " Phased-array measurements of full-scale military jet noise," AIAA Paper 2014-3069 (2014).

[7] K. L.Gee, M. Akamine, K. Okamoto, T. B. Neilsen, S. Tsutsumi, S. Teramoto, T. Okunuki, and M. Cook, " Characterization of supersonic laboratory-scale jet noise with vector acoustic intensity," AIAA Paper 2017-3519 (2017).

[8] D. F. Long, " Jet noise source location via acoustic holography and shadowgraph imagery," AIAA Paper 2008-2888 (2008).

[9] D. F. Long, " Evaluation of jet and shock cell noise via acoustic holography," AIAA Paper 2008-0005 (2008).

[10] P. N. Shah, H. Vold, and M. Yang, " Reconstruction of far-field noise using multireference acoustical holography measurements of high-speed jets," AIAA Paper 2011-2772 (2011).

[11] M. Lee and J. S. Bolton, " Source characterization of a subsonic jet by using near-field acoustical holography," J. Acoust. Soc. Am. **121**, 967-977 (2007).

[12] H. Vold, P. N. Shah, J. Davis, P. G. Bremner, D. McLaughlin, P. Morris, J. Veltin, and R. McKinley, " High-resolution continuous scan acoustical holography applied to high-speed jet noise," AIAA Paper 2010-3754 (2010).

[13] A. T. Wall, K. L. Gee, T. B. Neilsen, D. W. Krueger, and M. M. James, " Cylindrical acoustical holography applied to full-scale jet noise," J. Acoust. Soc. Am. **136**, 1120-1128 (2014).

[14] C. Tinney and P. Jordan, " The near pressure field of co-axial subsonic jets," J. Fluid Mech. **611**, 175-204 (2008).

[15] M. Mancinelli, T. Pagliaroli, A. Di Marco, R. Camussi, and T. Castelain, " Wavelet decomposition of hydrodynamic and acoustic pressures in the near field of the jet," J. Fluid Mech. **813**, 716-749 (2017).

[16] M. Akamine, Y. Nakanishi, K. Okamoto, S. Teramoto, T. Okunuki, and S. Tsutsumi, " Acoustic phenomena from correctly expanded supersonic jet impinging on inclined plate," AIAA J.**53**, 2061-2067 (2015).

[17] B. Greska, " Supersonic jet noise and its reduction using microjet injection," Ph.D. thesis, The Florida State University, FAMU-FSU College of Engineering, 2005.

[18] C. K. W. Tam, K. Viswanathan, K. K. Ahuja, and J. Panda, " The sources of jet noise: experimental evidence," J. of Fluid Mech. **615**, 253-292 (2008).

[19] A. B. Vaughn, T. B. Neilsen, K. L. Gee, K. Okamoto, and M. Akamine, " Near-field spatial variation in similarity spectra decomposition of a Mach 1.8 laboratory-scale jet," Proc. Mtgs. Acoust. **29**, 045004 (2016).

[20] R. Camussi, A. Di Marco, and T. Castelain, " Statistical analysis of the hydrodynamic pressure in the near field of compressible jets," Int. J. Heat Fl. **64**, 1-9 (2017).

[21] P. Jordan and T. Colonius, " Wave packets and turbulent jet noise," Annu. Rev. Fluid Mech. **45**, 173-195 (2013).